Multi-decadal changes in the South China Sea mixed layer salinity

Lili Zeng[1,3*], Eric P. Chassignet[2], Xiaobiao Xu[2] and Dongxiao Wang[1*]

1. State Key Laboratory of Tropical Oceanography (LTO), South China Sea Institute of Oceanology, Chinese Academy of Sciences, Guangzhou, 510301, China

2. Center for Ocean-Atmospheric Prediction Studies, Florida State University, Tallahassee, Florida, USA

3. Southern Marine Science and Engineering Guangdong Laboratory (Guangzhou), 511458, China.

Revised manuscript for the Climate Dynamics

Corresponding Author:
Dr. Lili Zeng
Dr. Dongxiao Wang
State Key Laboratory of Tropical Oceanography, South China Sea Institute of Oceanology, Chinese Academic of Sciences, Guangzhou, China

Tel: (86) 20- 8902-4304; Fax: (86)20-8902-4304
Email: zenglili@scsio.ac.cn; dxwang@scsio.ac.cn

Abstract

A recently assembled South China Sea Physical Oceanographic Dataset (SCSPOD) provides the first observational evidence for mixed layer salinity changes in the South China Sea (SCS) from 1960 to 2015. During this period, the mixed layer waters freshened by 0.22 psu. The mixed layer salinity variability is found to be in sync with the Pacific Decadal Oscillation (PDO); it freshened in the 1960s, started to salinify in 1974, freshened again from 1993, and then salinified once again from 2012, with linear trends of –0.019, 0.020, and –0.024 psu/yr, respectively. A box-average salinity budget analysis shows that the surface forcing, horizontal advection, and vertical entrainment terms together can, to a large degree, explain the observed trend in mixed layer salinity. The mixed layer freshening is driven by weakened surface fresh water loss and saline water transport, while salinification is associated with enhanced surface freshwater loss and salt transport through the Luzon Strait. The long-term mixed layer salinity changes affect the stratification, inducing a thinner mixed layer and stronger barrier layer during freshening periods that favor stronger regional ocean–atmosphere interaction.

Key words: South China Sea; mixed layer salinity; long-term variability

1. Introduction

The global water cycle is a key element of the climate system, yet it is poorly understood primarily because most of it occurs over the vast and under-sampled oceans (Schmitt, 1995; 2008). There is, however, ample evidence from salinity observations and numerical results from climate models indicating that the water cycle has changed over the past six decades (Wong et al., 1999; Munk, 2003) and that it has intensified (Durack et al., 2012).

Ocean salinity is globally conserved and quantification of its variability is essential to understanding the linkages between the water cycle and climate change (Curry et al., 2003; Boyer et al., 2005; Schmitt and Blair, 2015). Salinity measurements are used to diagnose changes in important components of the earth climate dynamics, such as surface freshwater flux, freshwater transport, and ocean mixing (Lukas and Lindstrom, 1991; Wijffels et al., 1992; Dickson et al 2002; Li et al, 2016ab). Robust and spatially coherent trends in salinity are found in the global ocean, where surface salinity increases are observed in evaporation-dominated regions and decreases are observed in precipitation-dominated regions (Durack et al., 2010; Skliris et al., 2014).

An abundance of historical records combined with recent observations from various programs have been used to document salinity changes throughout the globe. Long hydrographic records show that the salinity changes in the North Atlantic can be associated with significant changes in the North Atlantic Oscillation index (Dickson et al., 2002; Häkkinen, 2002; Curry et al., 2003; Holliday et al., 2008; Sarafanov et al.,

2008). Combined surface measurements document Pacific Decadal Oscillation (PDO)-like signals in sea surface salinity in the tropical Pacific (Delcroix et al., 2007; Du et al., 2015; Nan et al., 2015). Recent observations in the Southern Indian Ocean show a fast freshening since 1995 with a particularly striking acceleration since 2006 (Anilkumar et al., 2015; Menezes et al., 2017; Du et al., 2015).

The South China Sea (SCS) is the largest tropical marginal sea and has one of the lowest average surface salinity levels (~33 psu) (Zeng et al., 2014). It is located in the Indo-Pacific Ocean, identified by Durack et al. (2012) as one of the areas that experienced the most significant freshening during the 1950-2000 period. The temperature and salinity variations and controlling factors in the SCS are remarkably different from those in the open ocean. The South China Sea Throughflow (SCSTF) connects the Pacific and Indian Oceans, acts as an oceanic bridge, and strongly affects the heat and freshwater budgets in the SCS (Qu et al., 2006; Wang et al., 2006; Liu et al., 2012; Gordon et al., 2012). The SCSTF consists of inflow through the Luzon Strait and outflows through the Karimata, Mindoro, and Taiwan Straits, respectively (Figure 1). The large quantity of saline water brought through the Luzon Strait by the SCSTF can contribute as much salinity variations in the SCS as the local freshwater flux.

Due to the limited amount of observations, only a few studies have focused on salinity changes in the SCS and most of the attention has been on the northern SCS (Liu et al., 2012; Nan et al., 2013, 2016; Zhao et al., 2014; Zeng et al., 2014, 2016). Nan et al. (2013, 2016) showed that the freshening in the northeastern SCS in the 1990s and

2000s was associated with a weakening trend of the Kuroshio intrusion. Zeng et al. (2014) also found that the extreme freshening event in the northern SCS during 2012 was caused by a weak Kuroshio intrusion. Year 2012 is also when a 20-year freshening trend was reversed (Zeng et al., 2018). Decadal variability has been documented for subsurface salinity in the northern SCS during 1960 and 2012 (Zeng et al., 2016a). Finally, Liu et al. (2012) and Zhao et al. (2014) showed decadal changes in intermediate waters along 18°N in the northern basin (Liu et al., 2012; Zhao et al., 2014). However, very little is actually known about the decadal and long-term variability for the SCS as a whole.

In this paper, we analyze a recent observational dataset with the aim of 1) understanding the decadal and longer-term upper salinity changes in the SCS over the past six decades and 2) assessing the factors that contribute to these changes using a box-average mixed layer salinity budget analysis. The paper is organized as follows. The data and variables used to compute the budget are presented in section 2. The observed changes in salinity over the period 1960–2015 and the possible influence of the PDO are presented in section 3. In section 4, the box-average mixed layer salinity budget and the possible factors controlling variations in the mixed layer salinity are documented. Finally, conclusion and discussions are given in section 5.

2. Data and variables

2.1 In situ observational dataset

The South China Sea Physical Oceanographic Dataset (SCSPOD14) consists of

validated in situ observations collected from the World Ocean Database 2009 (WOD09), Argo floats, and the South China Sea Institute of Oceanology (SCSIO) measurements for the period 1919–2014 (Zeng et al., 2016b). This dataset has been updated by adding quality-controlled Argo float and SCSIO cruise measurements from 2015 (hereafter, SCSPOD15). Details of the data sampling characteristics, processing method, and quality control of this dataset can be found in Zeng et al. (2016b). We focus on the 1960-2015 period because the spatial and temporal coverage of the observations is dense enough to document variability. Overall, 34,485 records located deeper than 50 m within the well-sampled region (107–121°E, 3–23°N) are used for the analysis (Figure 2a). The spatial distributions of the observations as a function of longitude and latitude are shown in Figure 2b and 2c, as well as their sources: WOD09, Argo, and SCSIO. There are no salinity observations in SCSPOD15 for the year 2003, and several years in the mid-1960s have few observations. The interior basin (110–120°E) and northern basin (15–23°N) are sampled quite well with only a few years of poor data coverage. However, in the region west of 110°E and south of 15°N, the sampling is quite sparse between mid-1990s and mid-2000s. The mixed layer depth, mixed layer salinity, and barrier layer thickness are calculated for each profile as described in detail by Zeng et al. (2016b).

2.3 Variables

To assess the impact of the air-sea freshwater flux (i.e., evaporation–precipitation–river runoff, $E–P–R$, positive freshwater flux indicates loss of freshwater from the

ocean), we use the evaporation data from the Objectively Analyzed air–sea Fluxes version 3 (OAFlux; Yu and Weller, 2007) together with four precipitation products: the Precipitation Reconstruction (PREC; Chen et al., 2002), the National Centers for Environmental Prediction's Climate Prediction Center (CPC; Chen et al., 2002), the Global Precipitation Climatology Project version 2.3 (GPCP; Adler et al., 2003), and the Tropical Rainfall Measuring Mission 3B43 (TRMM; Huffman et al., 2007). The four net freshwater *E-P* flux datasets are hereafter referred to as PRECflux, CPCflux, GPCPflux, and TRMMflux, respectively. The Mekong and Pearl river runoffs are estimated from the river-basin-integrated precipitation as in Zeng et al. (2014).

To assess the impact of the horizontal salt transport, ocean currents from several products are used. They include the Simple Ocean Data Assimilation (SODA version 2.2.4, 1/2° spatial resolution) monthly reanalysis data from 1960 to 2012 (Carton et al., 2008), the National Centers for Environmental Prediction (NCEP) Global Ocean Data Assimilation System (GODAS, 0.333° latitude and 1° longitude spatial resolution) monthly reanalysis data from 1980 to 2012 (Huang et al., 2010), daily reanalysis data from 1993 to 2015 from the Hybrid Coordinate Ocean Model (HYCOM) data assimilative system GOFS 3.1 (HYCOM + NCODA Global 1/12° Analysis, Chassignet et al., 2009; Metzger et al., 2014), monthly outputs from the quasi global OGCM for the Earth Simulator (OFES, 1/2° spatial resolution) hindcast simulation driven by daily mean wind stress of the NCEP/NCAR reanalysis data from 1960 to 2010 (Sasaki et al., 2008), and 3-day mean West Pacific (including the SCS) hindcast data from 1992 to

2015 using the Regional Ocean Modeling Systems (ROMS, 1/8° spatial resolution; Xiu et al., 2010). These reanalysis and model datasets all show similar multi-decadal variations of upper layer salinity in the SCS. Finally, to assess the vertical entrainment, we use NCEP wind stress, OFES vertical velocity outputs, and mixed layer depth calculated from SCSPOD15 profiles.

3. Observed features

3.1 Salinity change between 1960 and 2015 (56 years)

We start by first looking at the long-term salinity change in the upper 250 m from 1960 to 2015 (56 years). The longitudinally and latitudinally averaged salinity changes in the SCS for the upper 250 m were obtained using SCSPOD15 and its variability are displayed in Figures 3a and 3b. Note that shallow regions less than 250 m are not include in the average. Between 1960 and 2015, the salinity in the upper 50 m is marked by a significant long-term decrease of 0.22 psu in salinity (Fig 3a), with an averaged trend of -0.20 psu/50yr. This freshening trend can extend as far down as 100 m in the western SCS. In the east, the freshening near the Luzon Strait is even deeper extending as far down as 250 m. The freshening in the upper 100 m is also robust in the latitudinally averaged section, especially in the northern and central basin (Fig 3b). Below the freshening upper layer, both longitudinally and latitudinally averaged salinity changes show an apparent subsurface salinification beneath 100 m in the central basin (Figs 3a and 3b). Figure 3c gives the basin-wide averaged profile of salinity changes from 1960 to 2015 in the SCS. The profile shows that the SCS experienced a

180 significant freshening in the top 100 m and weak salinification in the subsurface layers
181 (Fig 3c). Regions where the freshening magnitude exceeds 0.20 psu/50yr are limited to
182 the mixed layer waters.

183 The linear trends in mixed layer salinity are calculated on 2°×2° bins and are
184 displayed in Figure 4. The crosses indicate the bins in which the computations of trends
185 are not reliable using a Mann-Kendall test. Overall, the mixed layer salinity in the SCS
186 has been decreasing over the past 56 years, with an averaged trend of -0.15 psu/50yr
187 (or -0.003 psu/yr). In the northeastern region, the long-term freshening trend is about -
188 0.175psu/50yr. This trend is comparable to the value east of the Luzon Strait reported
189 by Durack et al. (2012), i.e., -0.15 to -0.20 psu over a 50-year period (1950–2000). The
190 freshening trend is weaker in the southern part of the basin than in the northern basin.
191 Note that we cannot clearly state how much of the spatial pattern in the southern basin
192 is due to less observational data distribution. But at the present stage, it will provide
193 valuable observational spatial salinity changing information in the SCS.

194 **3.2 Decadal variability**

195 The decrease in mixed layer salinity between 1960 and 2015 is not necessarily
196 linear; freshening during one time period could alternate with salinification during
197 another. To explore the decadal variability, we first show in Figure 5 the temperature-
198 salinity (T–S) diagram averaged basin-wide for each of the six decades. These *T*–*S*
199 curves are an effective way to distinguish freshening or salinification periods (decades)
200 from the climatological mean conditions. They show that the SCS has experienced

significant decadal variability over the past six decades. The upper ocean salinity is highest in the 1990s and lowest in the 2010s. The great salinification of the 1990s also occurred in the Atlantic, tropical Pacific, and Indian Ocean (Curry et al., 2003; Delcroix el al., 2007; Skliris et al., 2014). These decadal differences can be seen in all of the datasets (WOD09, SCSIO, and Argo) that comprise SCSPOD15. Different datasets show important similarities in the decadal changes over the past sixty years. Except that the saltier water brought by Argo floats from the western Pacific cause the difference between Argo and SCSIO in 2010s in certain degree (Figure 5c and 5d).

To further illustrate the variability of the salinity in the SCS, in Figure 6a we plot yearly variations of basin-wide averaged salinity for the upper 250 m from 1960 to 2015. The upper ocean started to freshen in the 1960s and continued through the mid-1980s. This was followed by a short salinification period in the late 1970s, then freshening again until the mid-1990s. Significant freshening occurred yet again in the 2010s. This variability, which can be as high as 0.4 psu, is clearly visible in the salinity anomaly plot (Figure 6b), with phases of high salinity in the 1960s and mid-1990s and low salinity in the mid-1970s and the 2010s. The salinity anomalies can extend down from the surface to about 200 m, but the highest anomalies with amplitude of up to 0.4 psu are mostly confined to the mixed layer. We therefore now focus on the mixed layer salinity variability.

3.3 Mixed layer salinity variability

Figure 7 shows longitude–time sections of mixed layer salinity from 1960 to 2015

averaged between 3°N and 23°N. There is a striking difference between the SCS and Pacific waters east of 121°E. The mixed layer salinity in the SCS is significantly lower than that of Pacific waters. As discussed in the previous section, the mixed layer salinity underwent freshening in the 1970s, salinification during the 1980s and 1990s (~0.4 psu), and then freshening again. The lowest salinity was recorded in 2012 (Zeng et al., 2014). This is summarized by Figure 8, which shows the temporal evolution of the basin-wide mixed layer salinity, including the one standard errors. The error bar is estimated as the standard error of all mixed layer salinity values for a given calendar year. The seven-year band pass time series (in blue) can be divided into four periods separated by three mixed layer salinity minima and maxima: 1974 (the secondary minimum mixed layer salinity), 1993 (the maximum mixed layer salinity), and 2012 (the minimum mixed layer salinity). The observed change in mixed layer salinity was first a decrease of about –0.4 psu during 1960–1974. The mixed layer salinity then increased by ~0.6 psu between 1974 and 1993, followed by a sharp decrease of ~0.7 psu between 1993 and 2012. It increased again after 2012. The corresponding linear trends are –0.020, 0.019, and –0.024 psu/yr, about one order of magnitude higher than the 56-year long-term trend (–0.004 psu/yr). All trends reported here are statistically significant according to the *t*-test. The salinity change rates in the mixed layer are about two to three times higher than those reported for the subsurface layer by Zeng et al (2016a).

To explore the regional differences in mixed layer salinity variability, yearly variations in the mixed layer salinity anomaly averaged over six well-sampled regions

are shown in Figure 9. The decadal timescale variability is similar for each region with a salinification period that is slightly more noticeable in the northern basin than in the southern basin.

3.4 Mixed layer salinity variability and the PDO

As the largest marginal sea in the northwest Pacific Ocean, the climate and environment of the SCS are strongly influenced by the PDO. For example, a coral geochemistry record in the northern SCS was reported to be significantly correlated with the PDO index over the last century (Deng et al., 2013). In Figure 10, we superimpose the mixed layer salinity anomaly on the PDO index and find that there is a reasonably good agreement between the two curves.

The correlation between yearly mean mixed layer salinities and the PDO index is 0.45 at the 95% confidence level. Their correlation is much higher after the 1990s (0.52) than prior (0.19). The freshening periods generally coincide with a declining stage of the PDO index, while the salinification periods are associated with an ascending stage. The largest change in PDO index and mixed layer salinity occurs after 2012 when both the mixed layer salinity and the PDO index rise quickly. This salinification from late 2012 occurs when the phase of PDO switches from negative to positive has been discussed in detail in our previous work (Zeng et al., 2018)

4. Factors controlling variations in the mixed layer salinity

What are the reasons for the salinification and freshening in the SCS mixed layer

salinity? In general, factors that can cause the mixed layer salinity changes include a) net air-sea freshwater flux, b) the Luzon Strait transport induced horizontal salt advection, and c) vertical entrainment and small-scale mixing processes. In this section, we focus on the change in the surface freshwater flux and the surface current during salinification/freshening periods (4.1); we then provide a more quantitative assessment for each factor that contributes to the observed salinity change (4.2 and 4.3).

4.1 Dry/wet conditions during salinification/freshening periods

Figure 11a displays the spatial distribution of the long-term (1960–2015) mean net surface freshwater flux (color shading) based on the GPCP and mixed layer circulation (vectors) based on the OFES model simulation. GPCPflux dataset and the OFES surface velocities are shown here because of their good spatio-temporal coverage in the SCS. Over the 56-year period (Figure 11a), evaporation is lower than precipitation in the SCS, except to the southwest of Taiwan. There is also a clear signature of the Kuroshio intrusion across the Luzon Strait in the SCS circulation.

Figures 11b-c show the change in the surface freshwater flux and the mixed layer current for a salinification period (1974-1993) and a freshening period (1993-2012). During the 1974-1993 salinification period (Figure 11b), the increasing trend of freshwater loss dominated almost everywhere, except for the central northern SCS where the freshwater flux was negative. In the surface circulation, there is an anomalous westward flow trend east of the Luzon Strait (red vectors, Figure 11b) that, according to Yu and Qu (2013), is an indication of a northward shift of the North Equatorial

Current (NEC) bifurcation, suggesting a stronger Kuroshio intrusion or larger Luzon Strait transport. During the 1993-2012 freshening period (Figure 11c), the net freshwater flux and ocean current distribution were opposite to that of the 1974-1993 salinification period. There is a decreasing trend of net freshwater loss across almost the entire basin and the eastward flow trend east of the Luzon Strait was unfavorable for Kuroshio intrusion (black vectors, Figure 11c). In summary, the trends of enhanced (decreased) freshwater loss and Luzon Strait transport provided salinification (freshening) conditions during a salinification (freshening) period.

Previous studies have shown that the PDO has an important influence on Asian monsoon and monsoon precipitation. The PDO can either strengthen or weaken the Walker circulation over the Indo-Pacific Ocean depending on the phase of the PDO (Krishnamurthy and Krishnamurthy, 2014). For the SCS, during positive PDO phases the descending motion of the Walker circulation leads to drought conditions over the basin, while during negative phases the ascending motion brings heavy rainfall to the SCS. The net freshwater loss is generally above average during the ascent PDO stage and below average during the declining PDO stage, with exceptions occurring during the mid-1990s and 2000s (Figure 12). Du et al. (2015) also reported a reduction in freshwater loss in the southeastern tropical Indian Ocean starting from the mid-1990s due to intensified Walker circulation. Yu and Qu (2013) found a significant imprint of the PDO on decadal SCSTF variability. They indicated that during positive PDO phases, the NEC bifurcation shifts northward and is responsible for the southward intrusion of

the Aleutian low, leading to a weaker Kuroshio and stronger SCSTF in the upper 750 m. As shown in Figure 12, we find that the Luzon Strait transport integrated within the mixed layer is also closely related to the PDO index and, in the previous section, we showed that the averaged SCS mixed layer salinity variations are in sync with the PDO.

4.2 Box-average mixed layer salinity budget

In this section, we address whether the contribution of freshwater flux and Luzon Strait salt transport changes can fully account for the observed mixed layer salinity variations. In order to quantify the factors affecting the mixed layer salinity in the SCS, we perform a mixed layer salinity budget:

$$\underbrace{\frac{\partial S_m}{\partial t}}_{\text{Salinity tendency}} = \underbrace{\frac{S_0 \cdot (E-P-R) \cdot A_{SCS}}{V_{scs}}}_{\text{Surface forcing}} + \underbrace{\frac{T_{in} \cdot \Delta S_{in}}{V_{scs}} - \frac{T_{out} \cdot \Delta S_{out}}{V_{scs}}}_{\text{Horizontal advection}} - \underbrace{\frac{\Gamma(w_e) \cdot (S_m - S_b)}{H}}_{\text{Vertical entrainment}} + \varepsilon \quad (1)$$

From left to right, the terms correspond to mixed layer salinity tendency; surface forcing (loss from ocean defined as positive); horizontal advection term (defined as positive into the SCS), which contain advections into (second term on right side) and out of (third term) the basin; vertical entrainment; and a residual term, which includes diffusion and other small effects. Here, S_m is mixed layer salinity, S_o is the mean sea surface salinity, and A_{SCS}, H, and V_{SCS} are the surface area, mixed layer depth, and volume of the SCS (111°–121°E, 16°–22°N), respectively. E is the evaporation, P is the precipitation, and R is the river discharge; their net value is the net freshwater flux out of the basin (loss from the ocean is defined as positive).

Accurately quantifying the horizontal advection over the entire basin is difficult.

For a basin-wide study, the horizontal salinity transport can be represented by two components: inflow and outflow salt transport terms. Here, T_{in} and T_{out} are the volume transports into and out of the basin, respectively, and ΔS_{in} (ΔS_{out}) is the salinity difference between waters outside the inflow (outflow) straits and waters within the SCS, where a positive transport term means an enhanced salinity effect. As mentioned earlier, the exchange between the SCS and surrounding oceans consists mainly of inflow from the Kuroshio through the Luzon Strait, and outflow primarily through the Mindoro, Karimata, and Taiwan Straits (Yaremchuk et al., 2009). According to Qu et al. (2005), Song (2006) and Nan et al (2016), the freshwater exports across the outflow straits do not contribute much to the interannual SCS salinity budget, and we therefore did not take into account the freshwater export through the Taiwan, Mindoro and Karimata Straits.

The vertical processes contain vertical Ekman velocity and diapycnal mixing velocity (Michel et al., 2007). Following Michel et al. (2007) and Yu (2015), we have

$$w_e = w_{Ek} + w_m = \frac{\nabla \times \tau}{\rho f} + \left(\frac{\partial H}{\partial t} + \nabla \cdot HU \right) \quad (2)$$

where τ denotes wind stress, ρ the mixed layer density, f the Coriolis frequency, and U includes Ekman and geostrophic current. The Ekman velocity w_{EK} corresponds to the upwelling (downwelling) generated by the convergence (divergence) of the horizontal Ekman transport (Yu, 2011). The mixing velocity w_m, or the mixed layer depth tendency, can be influenced by wind, buoyancy, and other thermodynamic processes. In Eq. (1), Γ is the Heaviside function and w_e is the entrainment velocity at

346 the bottom of the mixed layer; S_b is defined as the salinity at 20 m below the mixed
347 layer depth (Ren et al., 2011); Γ is used to represent entrainment ($w_e > 0$) and
348 detrainment ($w_e < 0$) to the mixed layer. Only the entrainment of subsurface water
349 affects the mixed layer salinity; detrainment removes mixed layer water but does not
350 modify its salinity (Niiler and Kraus, 1977; Michel et al., 2007; Yu, 2015).

351 Thus, we have a simplified expression for the box-average mixed layer salinity
352 variation:

353 $$\frac{\partial S_m}{\partial t} = \frac{S_0 \cdot (E-P-R) \cdot A_{SCS}}{V_{scs}} + \frac{LST \cdot \Delta S_{lz}}{V_{scs}} - \frac{\Gamma(w_e) \cdot (S_m - S_b)}{H} + \varepsilon \quad (3)$$

354 where ΔS_{lz} is the salinity difference between two sides of the Luzon Strait, the Western
355 Pacific water east of the Luzon Strait (S_{WP}) and the SCS (S_{SCS}).

356 **4.3 Factors controlling the mixed layer salinity variability**

357 To quantify the impact of the uncertainties associated with different data products,
358 we use several datasets (introduced in Section 2) for the freshwater flux and the Luzon
359 Strait transport to calculate the contribution of the surface forcing and advection terms
360 to the salinity budget. The temporal evolution of the budget terms are displayed in
361 psu/yr in Figure 13. The surface forcing and the horizontal advection terms dominate
362 and the vertical mixing is smaller by one order of magnitude. The trends for each term
363 during the freshening and salinification periods, using the different datasets, are listed
364 in Table 1.

365 During the 1960–1974 freshening period, the trends in the surface forcing,
366 advection, and entrainment terms were –0.011, –0.006 and –0.0003 psu/yr, respectively.

Their total contribution was about –0.017 psu/yr, roughly equivalent to the change in mixed layer salinity of –0.020 psu/yr. This result indicates that the surface forcing and advection terms basically determined the freshening trend. It also suggests that the effect of horizontal advection through the Luzon Strait was of similar magnitude to that of the surface forcing term. During the 1974–1993 salinification period, the surface forcing, advection, and entrainment terms all exhibited positive trends, with values of 0.016, 0.004, and 0.0013 psu/yr, respectively. The sum of the three terms, 0.021 psu/yr, was very close to the observed salinification trend of 0.019 psu/yr. This salinification was driven by enhanced surface freshwater loss and salt transport through the Luzon Strait. In contrast to the 1960-1974 freshening period, the surface forcing term was the dominant factor contributing to this salinification trend. After the year of maximum salinity (1993), the surface forcing, advection, and entrainment terms decreased again with negative trends of –0.010, –0.010, and –0.0008 psu/yr, respectively. The total impact of –0.021 psu/yr was close to the observed freshening trend of –0.024 psu/yr. Similar as the 1960–1974 freshening period, the surface forcing and advection terms basically determined the 1993-2012 freshening period. Overall, though admittedly crude, this calculation was able to quantitatively account for most of the observed mixed layer salinity changes (Figure 13d). In summary, the mixed layer freshening was controlled by comparable contributions from the surface forcing and advection terms, while the surface forcing is the dominant term for mixed layer salinification.

5 Conclusion and Discussions

In this paper, we examine the long-term variability of the mixed layer salinity in the SCS over the past 56 years (1960–2015) using an in situ dataset (SCSPOD15) to document the variability and a box-average salinity budget to quantify the factors controlling these variations.

The mixed layer salinity exhibits significant variability on decadal and longer timescales. During the 1960-2015 period, the mixed layer salinity freshened by more than 0.2 psu, with an averaged trend of -0.20 psu/50yr (or -0.004 psu/yr). This freshening trend is stronger in the northern basin than in the southern basin. The in situ observations in the SCS show that it became fresher in the 1960s, started to salinify in 1974, freshened again from 1993, and then salinized yet again in 2012, with linear trends of –0.019, 0.020, and –0.024 psu/yr, respectively. The mixed layer freshening is controlled by comparable contributions from the surface forcing and advection terms, while the surface forcing is the dominant term for mixed layer salinification (Figure 14). These decadal salinity change rates in the mixed layer are about two to three times larger than those in the subsurface layer as reported by Zeng et al. (2016). We find that the long-term variability in mixed layer salinity is in sync with the PDO. During the ascent (declining) stage of the PDO, the ascending (descending) motion of the Walker circulation leads to flood (drought) conditions over the basin, along with less (more) intrusion of additional saline water by the Luzon Strait transport associated with a stronger (weaker) Kuroshio; this results in freshening (salinification) in the SCS (see schematic Figure 15).

409 Although the SCSPOD15 dataset provides unprecedented observational coverage
410 in the SCS, there are still gaps and insufficient and uneven observations in some years.
411 One of the largest uncertainties in the trends assessment comes from the assembled
412 observational dataset. However, because we find that the observed mixed layer salinity
413 variability is in good agreement with the variability derived from a box-average mixed
414 layer salinity budget, we are confident that the trends reported here are representative.
415 The mixed layer salinity budget analysis is then used to quantify the forcing factors
416 controlling long-term changes in mixed layer salinity. The results show that the
417 freshening period is associated with a reduction in both the surface freshwater loss and
418 the Luzon Strait transport advection terms, while salinification is associated with
419 enhanced surface freshwater loss and salt transport through the Luzon Strait. Note that
420 the mixed layer freshening is controlled by equal contributions from the surface forcing
421 and advection terms, while the salinification period is mostly controlled by enhanced
422 surface freshwater loss. While we have assessed the uncertainty by utilizing as many
423 surface forcing products and ocean current outputs as possible (both with and without
424 data assimilation), it is clear that the accuracy of different surface forcing products and
425 the realism of the ocean model current outputs remains an issue. In the simplified
426 salinity budget, the freshwater exports in the Taiwan, Mindoro and Karimata Straits
427 were not taken into account as the freshwater exports across the outflow straits does not
428 contribute much to the interannual SCS salinity budget (Qu et al., 2005, Song, 2006;
429 and Nan et al., 2016). However, there are freshwater inputs into the Indonesian Seas
430 that can influence the variability of Indonesian Throughflow (ITF) transport and induce

salinity changes in the eastern Indian Ocean (Gordon et al., 2003; Hu and Sprintall, 2016, 2017; Lee et al., 2019). Future studies could examine the potential influence of the freshwater outflows of the SCS on the ITF variations and related salinity changes.

Finally, the question as to whether the mixed layer salinity changes (freshening or salinification) can induce significant climate change in the SCS depends on the magnitude of the trends. Sufficiently large salinity changes will modify the ocean stratification and air-sea flux exchanges and, when exceeding a threshold, will impact the SCS thermohaline circulation and the climate (Manabe and Stouffer, 1995; Wu et al., 2004). Barreiro et al. (2008) showed that a freshwater input exceeding 0.3 Sv per decade (a model-dependent value) can weaken the thermohaline circulation in the North Atlantic. We are then led to ask what is the threshold that must be exceeded in the SCS to significantly influence its thermohaline circulation? In the SCS, changes in the mixed layer salinity regulate the mixed layer (Figure 16). The observed mixed layer salinity freshening or salinification trends could constructively contribute to a reduction or enhancement of the mixed layer density (Figure 16a). The shoaling or deepening of the mixed layer depth generally coincides with a freshening or salinification of the mixed layer salinity (Figure 16b). Variations in salinity stratification that forms a barrier layer have an important influence on climate (Maes et al., 2002, 2005). For the SCS, there was no significant change in the barrier layer during the salinification, but a shoaling mixed layer depth was associated with a slight increase in the barrier layer during the two freshening periods (Figure 16c). A combination of the relatively shallow mixed

452 layer and stronger barrier layer during the freshening period could lead to a
453 strengthening of the ocean–atmosphere coupling in the SCS. A realistic climate model
454 and well-designed experiments are needed to answer these questions. Future studies
455 could examine long-term changes in salinity, the threshold for major change, and
456 detailed processes affecting the thermohaline circulation and climate change.

457 **Acknowledgements:**

458 We benefited from several observational datasets and numerical results made freely
459 available, including the SCSPOD dataset
460 (https://figshare.com/s/e5327a334130cd44dc6a), the OAFlux evaporation
461 (ftp://ftp.whoi.edu/pub/science/oaflux/data_v3), the PREC precipitation
462 (http://www.esrl.noaa.gov/psd/data/gridded/data.prec.html), the CPC precipitation
463 (http://apdrc.soest.hawaii.edu/data/data.php), the GPCP precipitation
464 (http://www.esrl.noaa.gov/psd/data/gridded/data.gpcp.html), the TRMM 3B43
465 precipitation (http://mirador.gsfc.nasa.gov/cgi-bin/mirador/), OFES outputs
466 (http://apdrc.soest.hawaii.edu/data/data.php), the SODA
467 (http://sodaserver.tamu.edu/assim/), the GODAS
468 (http://www.esrl.noaa.gov/psd/data/gridded/data.godas.html), and the HYCOM
469 (http://hycom.org/dataserver/glb-reanalysis). LZ is supported by the National Natural
470 Science Foundation of China (Nos. 42076209, 41776025, 41776026), Key Special
471 Project for Introduced Talents Team of Southern Marine Science and Engineering
472 Guangdong Laboratory (Guangzhou) (GML2019ZD0306), the Rising Star Foundation

473 of the South China Sea Institute of Oceanology (NHXX2019WL0101) and the Pearl
474 River S&T Nova Program of Guangzhou (201906010051). EPC and XX are
475 supported by the NOAA Climate Program Office MAPP Program (award
476 NA15OAR4310088) and the NSF Physical Oceanography Program (award 1537136).
477
478

References:

Adler, R. F., G. J. Huffman, A. Chang, R. Ferraro, P. Xie, J. Janowiak, B. Rudolf, U. Schneider, S. Curtis, D. Bolvin, A. Gruber, J. Susskind, P. Arkin, and E. Nelkin (2003), The version-2 global precipitation climatology project (GPCP) monthly precipitation analysis (1979-present), J. Hydrometeor., 4, 1147-1167.

Anilkumar, N., Chacko, R., Sabu, P., & George, J. V. (2015). Freshening of Antarctic bottom water in the Indian Ocean sector of southern ocean. Deep Sea Research Part II Topical Studies in Oceanography, 118, 162-169.

Barreiro, M., Fedorov, A., Pacanowski, R., & Philander, S. G. (2008). Abrupt climate changes: how freshening of the northern Atlantic affects the thermohaline and wind-driven oceanic circulations. Annual Review of Earth & Planetary Sciences, 36(36), 33-58.

Boyer, T. P., S. Levitus, J. I. Antonov, R. A. Locarnini, and H. E. Garcia (2005), Linear trends in salinity for the World Ocean, 1955–1998, Geophys. Res. Lett., 32, L01604, doi:10.1029/2004GL021791.

Carton, J. A., and B. S. Giese (2008), A reanalysis of ocean climate using simple ocean data assimilation (SODA), Mon. Weather Rev., 136, 2999–3017.

Chassignet, E. P., Hurlburt, H. E., Smedstad, O. M., Halliwell, G. R., Hogan, P. J., & Wallcraft, A. J., et al. (2009). Global ocean prediction with the Hybrid Coordinate Ocean Model (HYCOM). Oceanography, 22(2), 64-75.

Chen, M. Y., P. P. Xie, J. E. Janowiak, and P. A. Arkin (2002), Global land precipitation: A 50-yr monthly analysis based on gauge observations, J. Hydrometeorol., 3, 249–

501 266.
502 Curry, R., Dickson, B., & Yashayaev, I. (2003). A change in the freshwater balance of
503 the Atlantic ocean over the past four decades. Nature, 426(6968), 826-829.
504 Delcroix, T., S. Cravatte, and M. J. McPhaden (2007), Decadal variations and trends in
505 tropical Pacific sea surface salinity since 1970, J. Geophys. Res., 112 (C3) :266-281
506 Deng, W., G. Wei, L. Xie, T. Ke, Z. Wang, T. Zeng, and Y. Liu (2013), Variations in the
507 Pacific Decadal Oscillation since 1853 in a coral record from the northern South
508 China Sea, J. Geophys. Res. Oceans, 118, 2358–2366, doi:10.1002/jgrc.20180.
509 Dickson, B., Yashayaev, I., Meincke, J., Turrell, B., Dye, S., & Holfort, J. (2002). Rapid
510 freshening of the deep north Atlantic ocean over the past four decades. Nature,
511 416(6883), 832-7.
512 Du, Y., Y. Zhang., Ming Feng., T. Wang., N. Zhang, and S. Wijffels (2015), Decadal
513 trends of the upper ocean salinity in the tropical Indo-Pacific since mid-1990s. Sci.
514 Rep. 5, 16050; doi: 10.1038/srep16050 (2015).
515 Durack P. J., and S. E. Wijffels, (2010), Fifty-year trends in global ocean salinities and
516 their relationship to broadscale warming J. Clim. 23, 4342–4362
517 Durack, P. J., S. E. Wijffels, and R. J. Matear (2012), Ocean salinities reveal strong
518 global water cycle intensification during 1950 to 2000, Science, 336(6080), 455–
519 458, doi:10.1126/science.1212222.
520 Gordon, A. L., R. D. Susanto, and K. Vranes (2003), Cool Indonesian throughflow as a
521 consequence of restricted surface layer flow, Nature, 425(6960), 824-828.
522 Gordon, A. L., B. A. Huber, E. J. Metzger, R. D. Susanto, H. E. Hurlburt, and T. R. Adi

(2012), South China Sea throughflow impact on the Indonesian throughflow, Geophys. Res. Lett., 39 (11):117-128

Häkkinen, S., (2002), Freshening of the Labrador Sea surface waters in the 1990s: Another great salinity anomaly? Geophys. Res. Lett., 29(24) 2232, doi: 10.1029/2002GL015243

Holliday, N. P., Hughes, S. L., Bacon, S., Beszczynska-Möller, A., Hansen, B., & Lavin, A., et al. (2008), Reversal of the 1960s to 1990s freshening trend in the northeast North Atlantic and Nordic Seas, Geophys. Res. Lett., 35(3), 3614

Hu, S., and J. Sprintall (2016), Interannual Variability of the Indonesian Throughflow: the Salinity Effect, Journal of Geophysical Research: Oceans, 121, 2596-2615.

Hu, S., and J. Sprintall (2017), Observed Strengthening of Interbasin Exchange via the Indonesian Seas Due to Rainfall Intensification, Geophysical Research Letters, 44(3), 1448-1456.

Huang, B. Y., Xue, Y., Zhang, D. X., Kumar, A., & Mcphaden, M. J. (2010). The NCEP GODAS ocean analysis of the tropical Pacific mixed layer heat budget on seasonal to interannual time scales. Journal of Climate, 23(18), 4901-4925.

Huffman, G. J., R. F. Adler., D. T. Bolvin., G. Gu., E. J. Nelkin., K. P. Bowman., Y. Hong., E. F. Stocker., and D. B. Wolff., (2007), The TRMM multi-satellite precipitation analysis: quasi-global, multi-year, combined-sensor precipitation estimates at fine scale. J. Hydrometeorol. 8 (1), 38-55.

Krishnamurthy, L., and Krishnamurthy, V. (2014). Influence of PDO on south Asian summer monsoon and monsoon–ENSO relation. Climate Dynamics, 42(9-10), 1-14.

545 Lau, K. M. (2009). East Asian summer monsoon rainfall variability and climate
546 teleconnection. Journal of the Meteorological Society of Japan, 70(1B), p211-242.
547 Lee, T., S. Fournier, A. L. Gordon, and J. Sprintall (2019), Maritime Continent water
548 cycle regulates low-latitude chokepoint of global ocean circulation, Nature
549 Communications, 10(1), 2103, doi:10.1038/s41467-019-10109-z.
550 Liu, C., Wang, D., Chen, J., Du, Y., & Xie, Q. (2012). Freshening of the intermediate
551 water of the South China Sea between the 1960s and the 1980s. Chinese Journal of
552 Oceanology and Limnology, 30(6), 1010-1015.
553 Liu, Q., Huang, R., & Wang, D. (2012). Implication of the South China Sea throughflow
554 for the interannual variability of the regional upper-ocean heat content. Adv. Atmos.
555 Sci., 29(1), 54-62.
556 Li, L. R. W. Schmitt, C. Ummenhofer, K. Karnauskis, 2016. North Atlantic Salinity as
557 a Predictor of Sahel Rainfall. Science Advances, 2, e1501588.
558 Li, L., R. W. Schmitt, C. Ummenhofer, K. Karnauskis, 2016. Implications of North
559 Atlantic Sea Surface Salinity for Summer Precipitation over the US Midwest:
560 Mechanisms and Predictive Value. J. Climate, 29, 3143-3159.
561 Lukas, R., & Lindstrom, E. (1991). The mixed layer of the western equatorial Pacific
562 Ocean. Journal of Geophysical Research Atmospheres, 96(S01), 3343-3358.
563 Maes, C., J. Picaut, and S. Belamari (2002), Salinity barrier layer and onset of El Nino
564 in a Pacific coupled model, Geophys. Res. Lett., 29 (24), 59-1–59-4
565 Maes, C., J. Picaut, and S. Belamari (2005), Importance of salinity barrier layer for the
566 buildup of El Nino, J. Clim., 18, 104–118

567 Manabe, S., and Stouffer, R. J. (1995). Simulation of abrupt climate change induced by
568 freshwater input to the north Atlantic Ocean. Nature, 378(6553), 165-167.
569 Menezes, V. V., Macdonald, A. M., Schatzman, C (2017) Accelerated freshening of
570 Antarctic Bottom Water over the last decade in the Southern Indian Ocean. Sci. Adv.
571 3, e1601426.
572 Michel, S., B. Chapron., J. Tournadre, and N. Reul (2007), Sea surface salinity
573 variability from a simplified mixed layer model of the global ocean. Ocean Science
574 Discussions, 4(1), 41-106.
575 Munk, W. (2003). Ocean freshening, sea level rising. Science, 300(5628), 2041-2043.
576 Nan, F., H. Xue, F. Chai, D. Wang, F. Yu, M. Shi, P. Guo, and P. Xiu (2013), Weakening
577 of the Kuroshio intrusion into the South China Sea over the past two decades, J.
578 Clim., 26, 8097–8110.
579 Nan, F., Yu, F., Xue, H., Zeng, L., Wang, D., & Yang, S., et al. (2016). Freshening of
580 the upper ocean in the South China Sea since the early 1990s. Deep Sea Research
581 Part I Oceanographic Research Papers, 118, 20-29.
582 Niiler, P. P. and E. B. Kraus, One-dimensional models of the upper ocean, in Modeling
583 and Prediction of the Upper Layers of the Ocean, edited by E. B. Kraus, Pergamon,
584 New York, 325 pp., 143–172, 1977.
585 Qu, T., Du, Y., & Sasaki, H. (2006). South China Sea throughflow: A heat and
586 freshwater conveyor. Geophysical Research Letters. 332 (23): 430-452
587 Qu, T., Du, Y., Meyers, G., Ishida, A., Wang, D., (2005). Connecting the tropical Pacific
588 with Indian Ocean through South China Sea. Geophys. Res. Lett. 32, L24609.

589 http://dx.doi.org/10.1029/2005GL024698.
590 Ren, L., K. Speer, and E. P. Chassignet (2011), The mixed layer salinity budget and sea
591 ice in the Southern Ocean, J. Geophys. Res., 116 (C8): 239-255.
592 Sarafanov, A., A. Falina, A. Sokov, and A. Demidov (2008), Intense warming and
593 salinification of intermediate waters of southern origin in the eastern subpolar North
594 Atlantic in the 1990s to mid-2000s, J. Geophys. Res., 113 (C12): 451-459.
595 Sasaki, H, M. Nonaka, Y. Masumoto, Y. Sasai, H. Uehara, and H. Sakuma (2007), An
596 eddy-resolving hindcast simulation of the quasi-global ocean from 1950 to 2003 on
597 the Earth Simulator. High Resolution Numerical Modeling of the Atmosphere and
598 Ocean, W. Ohfuchi and K. Hamilton, Eds., Springer, 157–185.
599 Schmitt, R. W., 1995. The ocean component of the global water cycle. U.S. National
600 Report to International Union of Geodesy and Geophysics, 1991–1994, Supplement
601 to Reviews of Geophysics, pp. 1395–1409.
602 Schmitt, R. W., 2008. Salinity and the Global Water Cycle. Oceanography, 21 (1), 12-
603 19.
604 Schmitt, R. W. and A. Blair, (2015). A River of Salt. Oceanography, 28 (1), 40-45
605 Skliris, N., Marsh, R., Josey, S. A., Good, S. A., Liu, C., & Allan, R. P. (2014). Salinity
606 changes in the world ocean since 1950 in relation to changing surface freshwater
607 fluxes. Climate Dynamics, 43(3-4), 709-736.
608 Song, Y. T. (2006), Estimation of interbasin transport using ocean bottom pressure:
609 Theory and model for Asian marginal seas, J. Geophys. Res., 111, C11S19,
610 doi:10.1029/2005JC003189.

611 Wang, B., Zhang, Y., & Lu, M. M. (2004). Definition of South China Sea monsoon
612 onset and commencement of the east Asia summer monsoon. Journal of Climate,
613 17(4), 699-710.
614 Wang, D., Q. Liu, R. X. Huang, Y. Du, and T. Qu (2006), Interannual variability of the
615 South China Sea throughflow inferred from wind data and an ocean data assimilation
616 product. Geophys. Res. Lett., 33 (14): 110-118.
617 Wijffels, S., Schmitt, R., Bryden, H. & Stigebrandt (1992), A. Transport of freshwater
618 by the oceans. J. Phys. Oceanogr. 22, 155–162.
619 Wong, A. P. S., Bindoff, N. L. & Church, J. L. (1999), Large-scale freshening of
620 intermediate waters in the Pacific and Indian Oceans. Nature 400, 440–443
621 Wu, P., R. Wood, and P. Stott (2004), Does the recent freshening trend in the North
622 Atlantic indicate a weakening thermohaline circulation? Geophys. Res. Lett., 31
623 (2) :2301
624 Xiu, P., F. Chai, L. Shi, H. J. Xue., and Y. Chao (2010), A census of eddy activities in
625 the South China Sea during 1993–2007. J. Geophys. Res., 115, C03012, doi:
626 10.1029/2009JC005657.
627 Yaremchuk, M., J. McCreary Jr., Z. Yu, and R. Furue, 2009: The South China Sea
628 throughflow retrieved from climatological data. J. Phys. Oceanogr., 39, 753–767
629 Yu, L., and R. A. Weller (2007), Objectively Analyzed Air–Sea Heat Fluxes for the
630 Global Ice-free Oceans (1981–2005). Bull. Ameri. Meteor. Soc., 88, 527–539.
631 Yu, L. (2015), Sea-surface salinity fronts and associated salinity-minimum zones in the
632 tropical ocean, J. Geophys. Res. Oceans, 120(6), 4205-4225.

633 Yu, K., and T. Qu (2013), Imprint of the Pacific Decadal Oscillation on the South China
634 Sea throughflow variability, J. Clim., 26(24), 9797–9805.
635 Zeng, L., W. T. Liu, H. Xue, P. Xiu, and D. Wang (2014), Freshening in the South China
636 Sea during 2012 revealed by Aquarius and in situ data, J. Geophys. Res. Oceans,
637 119(12), 8296-8314.
638 Zeng L., D. Wang., P. Xiu., Y. Shu., Q. Wang and J. Chen., 2016, Decadal variation and
639 trends in subsurface salinity from 1960 to 2012 in the northern South China Sea.
640 Geophysical Research Letter, 43, 12181–12189
641 Zeng, L., D. Wang., J. Chen., W. Wang., and R. Chen (2016b), SCSPOD14, a South
642 China Sea physical oceanographic dataset derived from in situ measurements during
643 1919–2014. Sci. Data, 3:160029 doi: 10.1038/sdata.2016.29
644 Zeng, L., Chassignet, E. P., Schmitt, R. W., Xu, X., and Wang, D. (2018). Salinification
645 in the South China Sea since late 2012: A reversal of the freshening since the 1990s.
646 Geophysical Research Letters, 45. 2744–2751
647 Zhao, D., W. Wang., H. Qin., Q. Mao., D. Wang., and R. Chen (2014), Decadal changes
648 of the intermediate water at 18°N in the South China Sea. Acta Oceanologica Sinica
649 (in Chinese), 36(9): 56-64
650
651
652
653
654
655

Table 1: Long-term trends of each term in equation (3) in the SCS during the periods 1960–1974, 1974–1993, and 1993–2012. Units: psu/yr.

Mixed layer salinity trend	**Surface forcing**	**Horizontal advection**	**Vertical entrainment**	**Sum of 3 terms**	**Observed trend**
1960-1974	CPC:-0.014 PREC:-0.008 Mean:-0.011	SODA: -0.007 OFES: -0.006 Mean: -0.006	-0.0003	-0.017	-0.020
1974-1993	CPC:0.016 PREC:0.016 Mean:0.016	SODA: 0.002 OFES: 0.004 Mean: 0.003	0.0013	0.020	0.019
1993-2012	CPC:-0.011 PREC:-0.010 GPCP:-0.009 TRMM:-0.013 Mean:-0.010	SODA: -0.005 OFES: -0.006 GODAS:-0.009 ROMS:-0.010 HYCOM:-0.017 Mean:-0.010	-0.0008	-0.021	-0.024

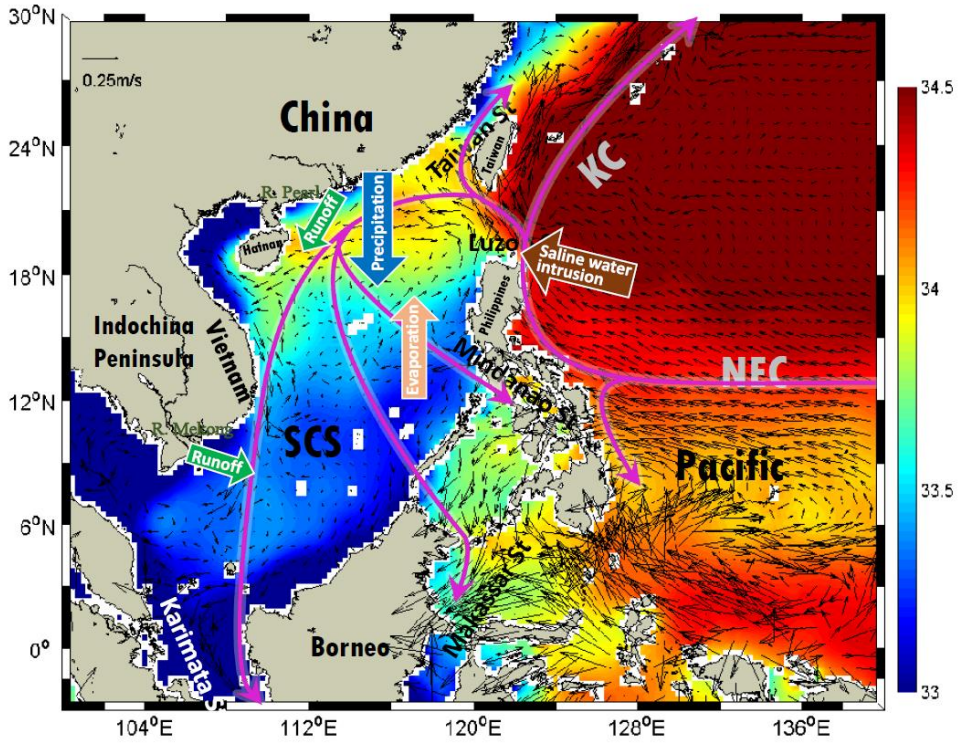

Figure 1. WOA mean surface salinity and OSCAR mean surface currents. Major currents in the SCS and adjacent waters are from Qu et al. (2006) and Hu et al. (2015), indicated by magenta lines. Abbreviations: SCS, South China Sea; NEC, North Equatorial Current; KC, Kuroshio Current.

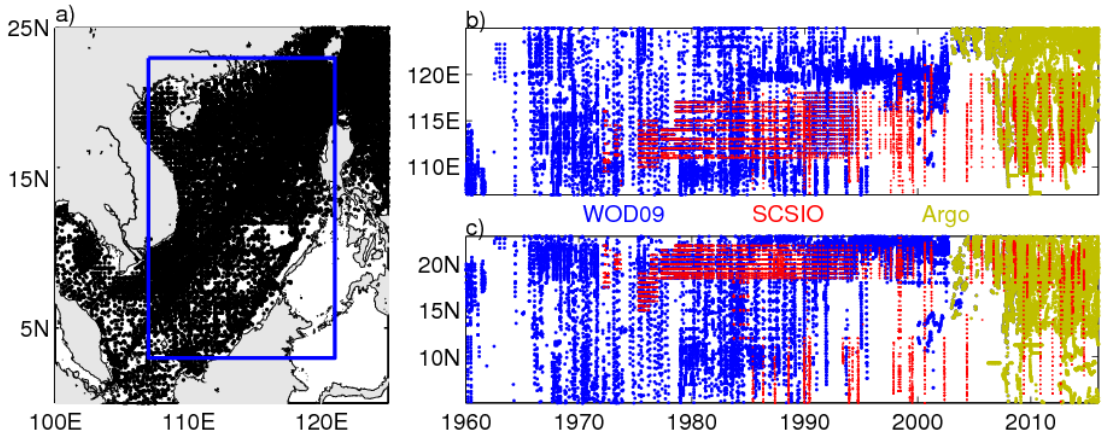

Figure 2. (a) Spatial distributions of observations from the SCSPOD15 dataset. The blue box represents the study area (SCS; 107–121°E, 3–23°N). (b) Longitude–time sections for the 3–23°N band of observations. (c) Latitude–time sections for the 107–121°E band of observations. The three data sources are marked by different colors: WOD09 (blue dots), SCSIO (red dots), and Argo (green dots).

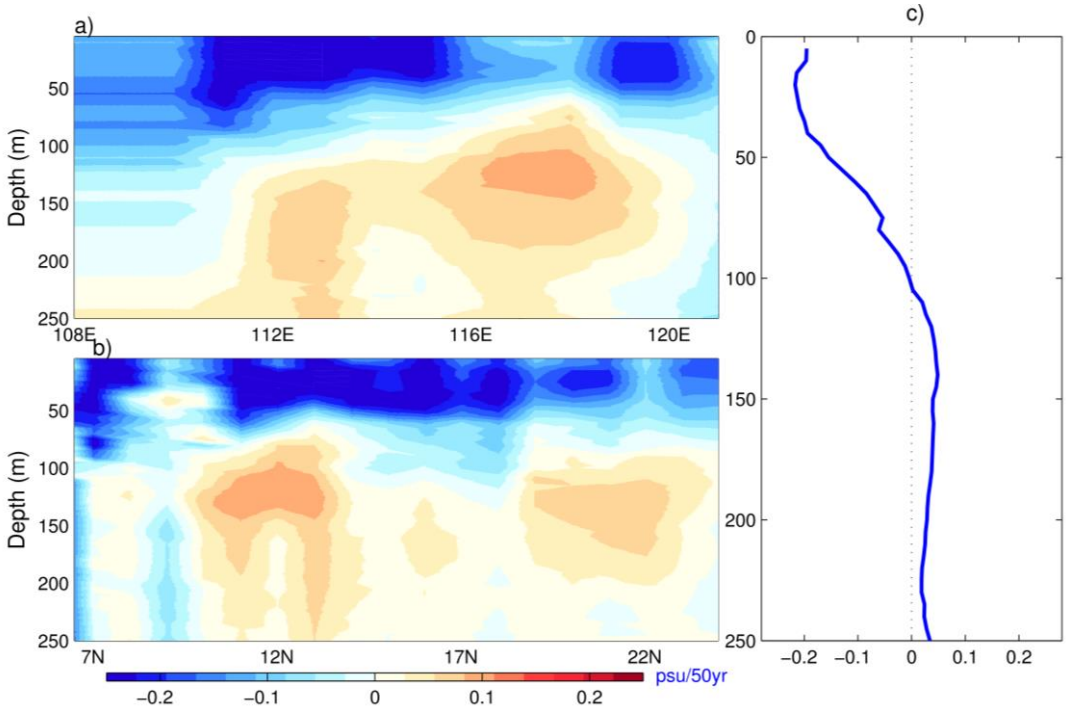

Figure 3. Vertical distributions of upper salinity change (psu/yr) from 1960 to 2015 in the SCS (basin area is defined as the region shown in Fig 2a). (a) Longitudinally average, (b) Latitudinally average, and (c) basin-wide average for the SCS. In order to compare with the trend identified by Durack et al. (2012), the unit is psu/50yr in this figure.

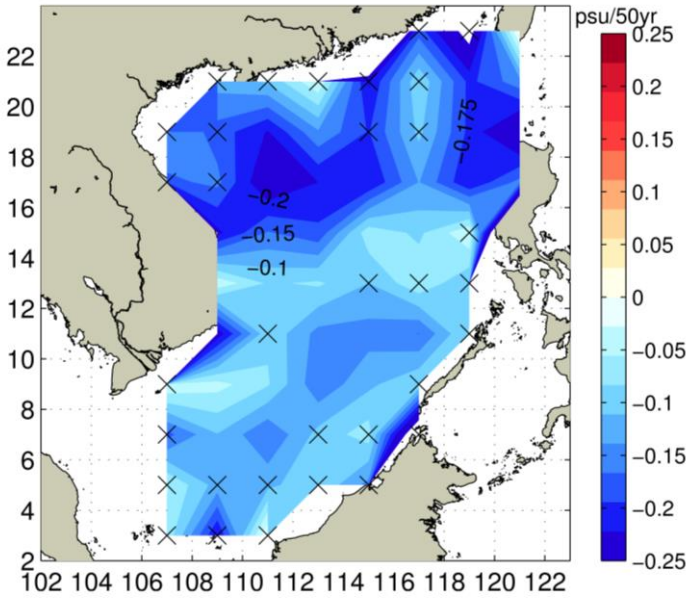

692

693 Figure 4. The linear trends in the mixed layer salinity calculated within each 2°×2°

694 bins in the SCS. The cross delimits bins where the calculations of trends are not
695 reliable in Mann-Kendall test. In order to compare with the trend identified by Durack
696 et al. (2012), the unit is psu/50yr in this figure.

697

698

699

700

701

702

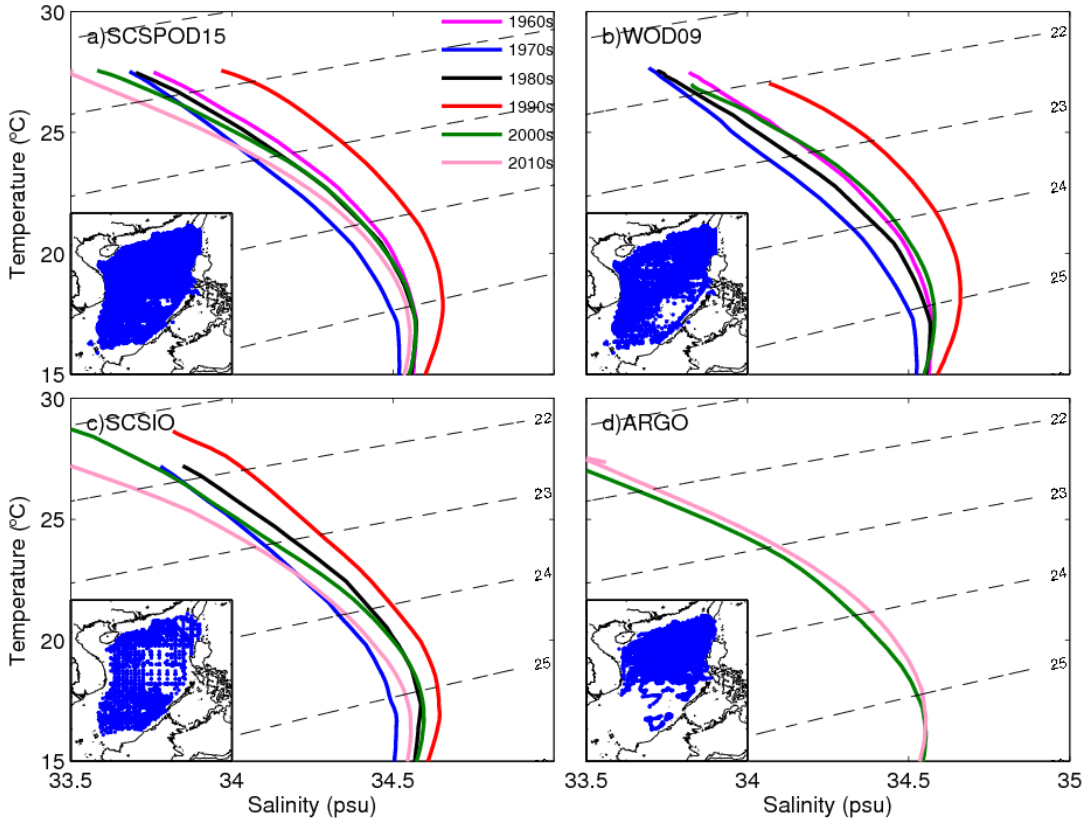

Figure 5. Decadal mean *T*–*S* curves from 1960 to 2015 in the upper SCS (1960s: magenta; 1970s: blue; 1980s: black; 1990s: red; 2000s: green; 2010s: pink) based on, (a) SCSPOD15; (b) WOD09; (c) SCSIO; (d) Argo.

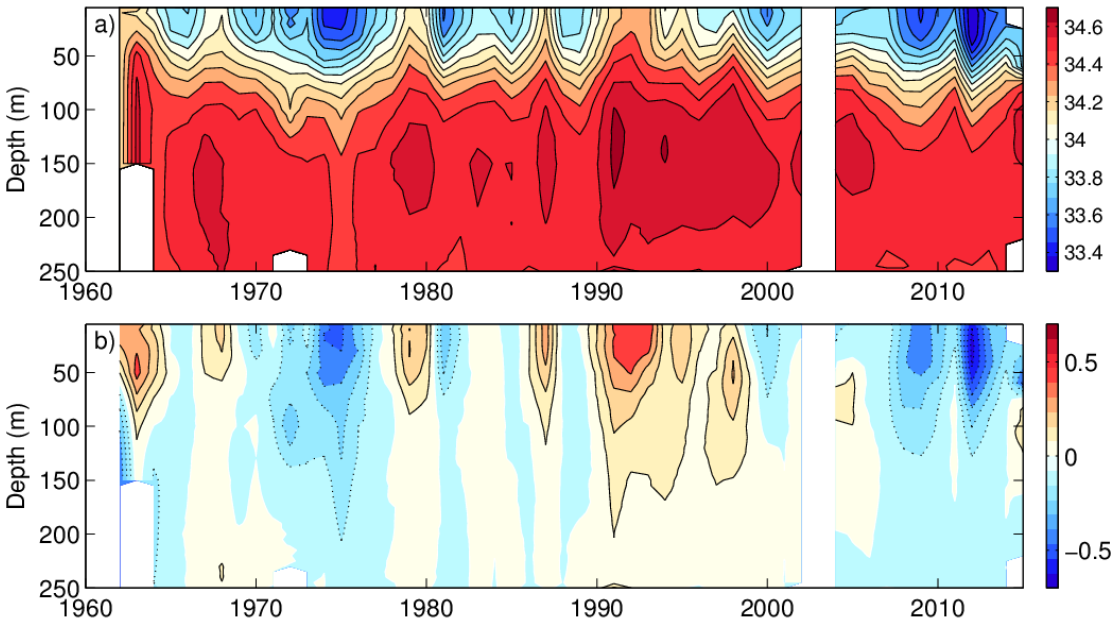

Figure 6. Time-depth sections of basin-wide averaged yearly mean (a) salinity, and (b) salinity anomalies (take off the temporal averaged yearly time-depth section, positive salinity anomaly: red; negative salinity anomaly: blue) in the upper SCS.

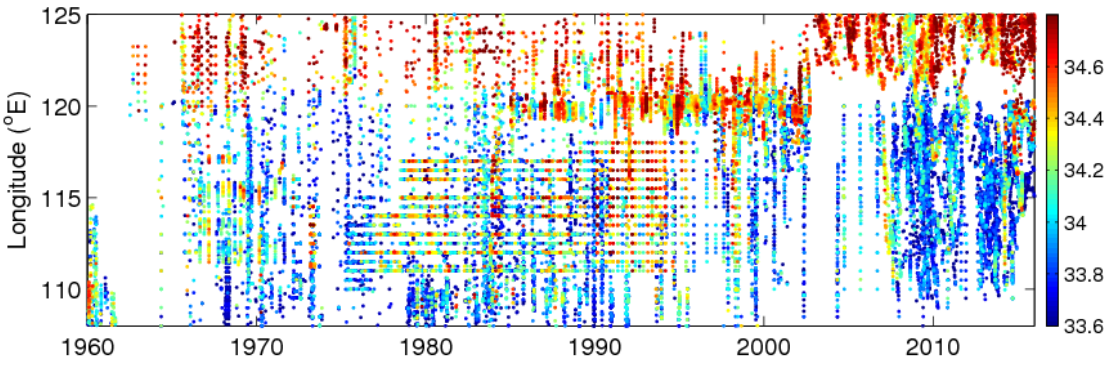

Figure 7. Longitude–time sections of mixed layer salinity (color, psu) for the 3–23°N band from 1960 to 2015 in the SCS.

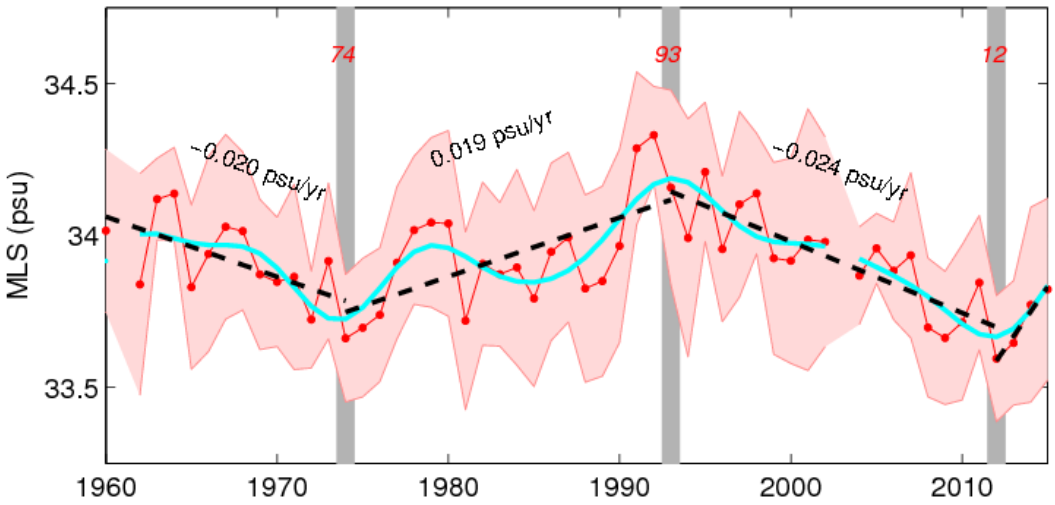

Figure 8. Time series of average yearly basin-wide mixed layer salinity from 1960 to 2015 in the SCS. Shading (light red) indicates error bars. The error bar is estimated as the standard error of all mixed layer salinity values for a given calendar year. The low-frequency curve (blue) represents the seven-year filtered values used to highlight long-term changes. The dashed line represents the linear least squares fit of the yearly values used to quantify linear trends (psu/yr). The gray shaded areas indicate turning points in 1974, 1993, and 2012.

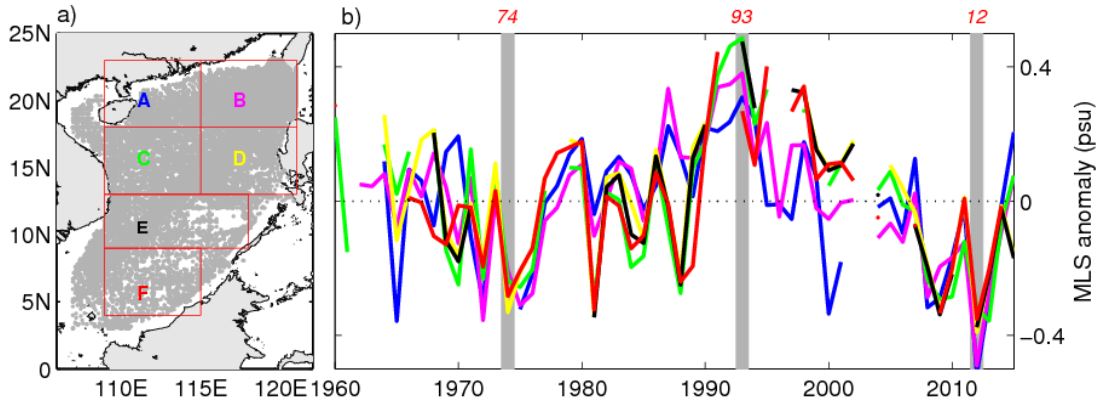

Figure 9. (a) Spatial distributions of selected SCSPOD15 observations in the study area (107–121°E, 3–23°N) and six selected areas (boxes) used for spatial averages. (b) Time series of yearly mixed layer salinity anomalies averaged in the six areas (take off the box-averaged yearly mixed layer salinity) from 1960 to 2015 in the SCS indicated by boxes in (a). The gray shaded areas indicate turning points in 1974, 1993, and 2012.

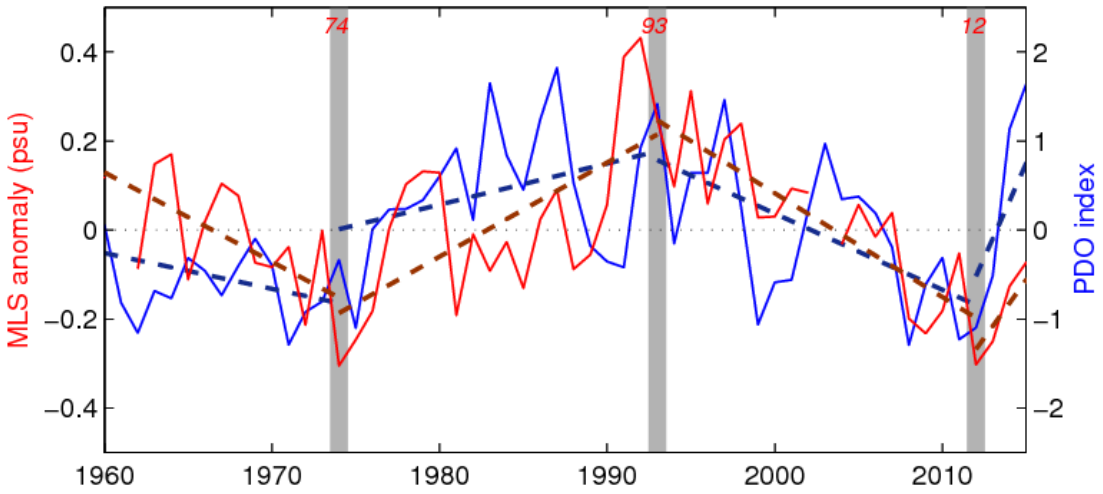

Figure 10. Time series of yearly PDO index (blue) and mixed layer salinity anomaly (take off the basin-averaged yearly mixed layer salinity, red) in the SCS from 1960 to 2015. The gray shaded areas indicate turning points in 1974, 1993, and 2012. The blue and red dashed line represents the linear least squares fit of the yearly values used to quantify linear trends for PDO and mixed layer salinity anomaly, respectively.

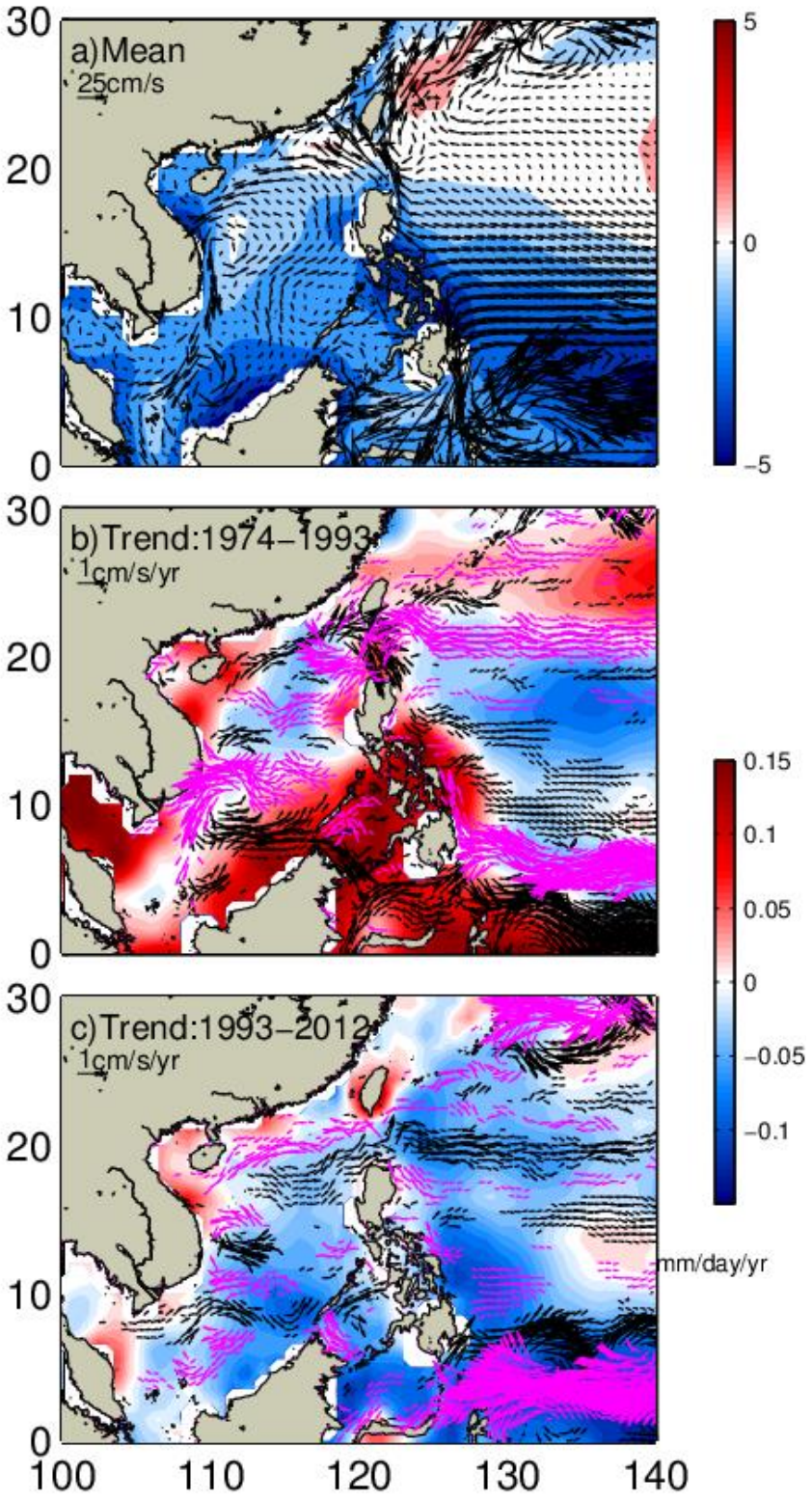

Figure 11. (a) Long-term mean GPCP freshwater flux (*E*–*P*, shading, unit: mm/d) and OFES mixed layer circulation (vectors, unit: cm/s). (b) Linear trend of GPCP freshwater flux (shading, unit: mm/d/yr) and OFES circulation from 1974 to 1993 (magenta vectors: westerly currents; black vectors: easterly currents; unit: cm/s/yr). (c) Same as (b), but for the period 1993 to 2012.

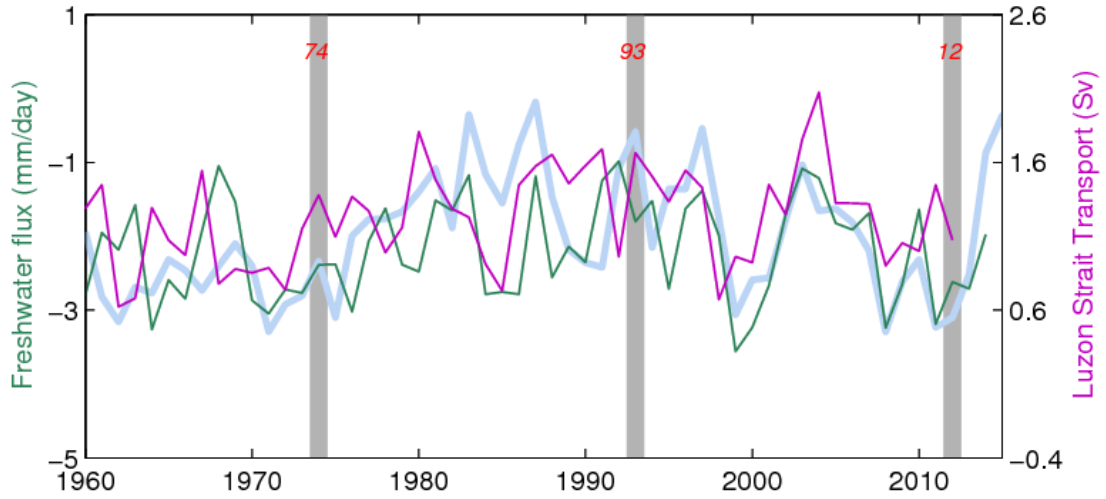

Figure 12. Time series of yearly PREC net freshwater flux (*E*–*P*, green, unit: mm/d), OFES Luzon Strait transport (purple, unit: Sv) and yearly PDO index (light blue, PDO-2 is shown). The gray shaded areas indicate turning points in 1974, 1993, and 2012.

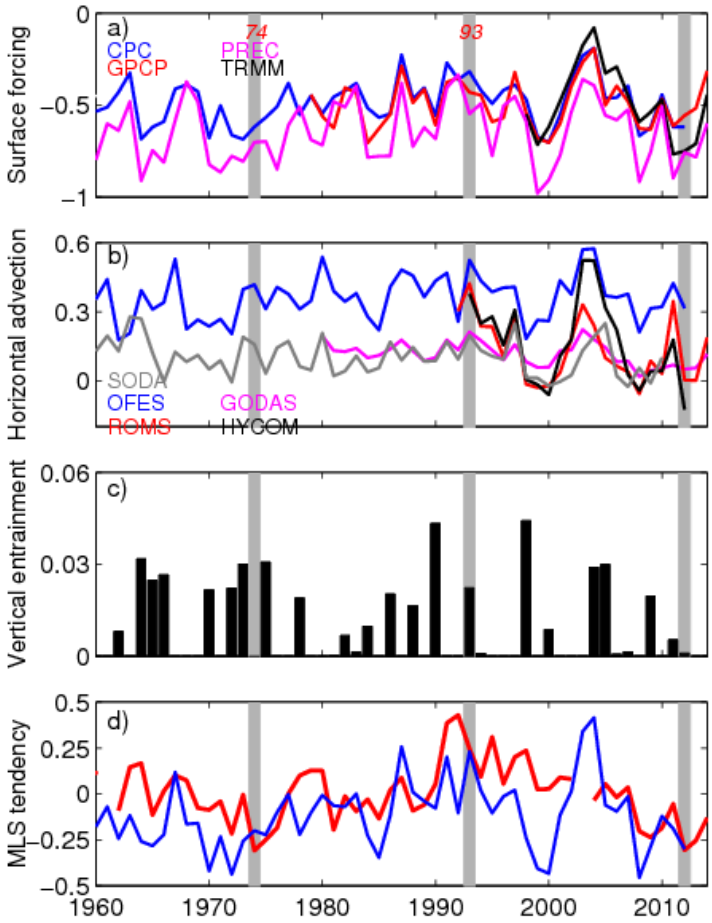

Figure 13. Spatial average of each term in equation (3) for the SCS (unit: psu/yr). (a) Net freshwater flux term (CPCflux: blue; PRECflux: magenta; GPCPflux: red; TRMMflux: black). (b) Luzon Strait transport induced horizontal advection term (SODAadv: gray; OFESadv: blue; GODASadv: magenta; ROMSadv: red; HYCOMadv: black). (c) Vertical entrainment term. (d) Mixed layer salinity tendency, and the sum of the freshwater flux, horizontal advection, and vertical entrainment terms.

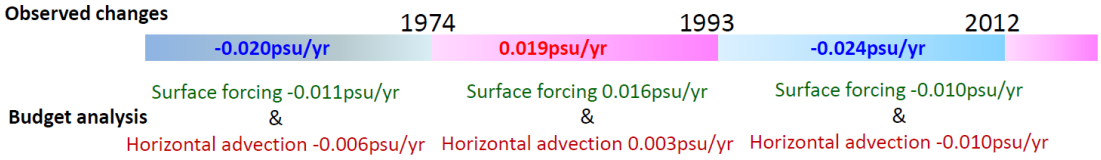

Figure 14. Schematic timeline of the observed salinity changes (shading bars) in the SCS during the periods 1960–1974, 1974–1993, and 1993–2012. The contribution of surface forcing and horizontal advection terms are given below. Units: psu/yr.

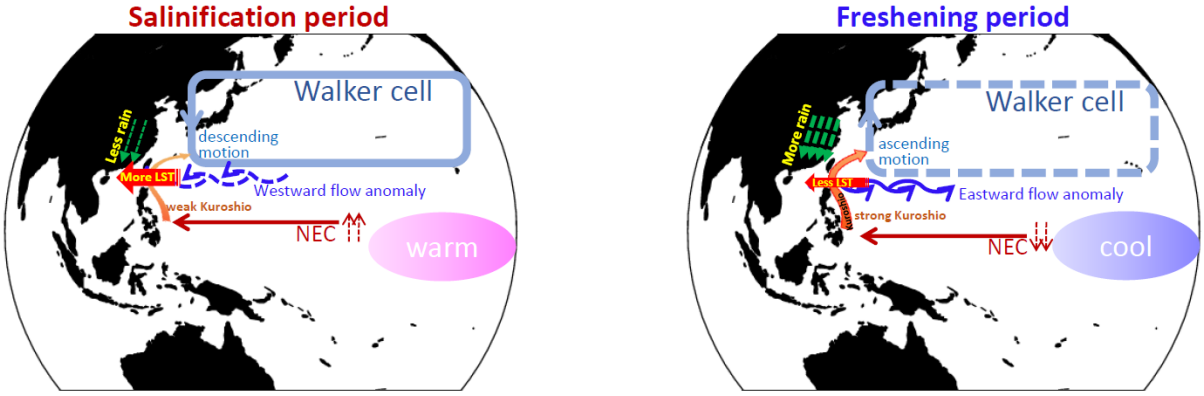

Figure 15. Schematic diagram of the (a) salinification and (b) freshening periods in the SCS.

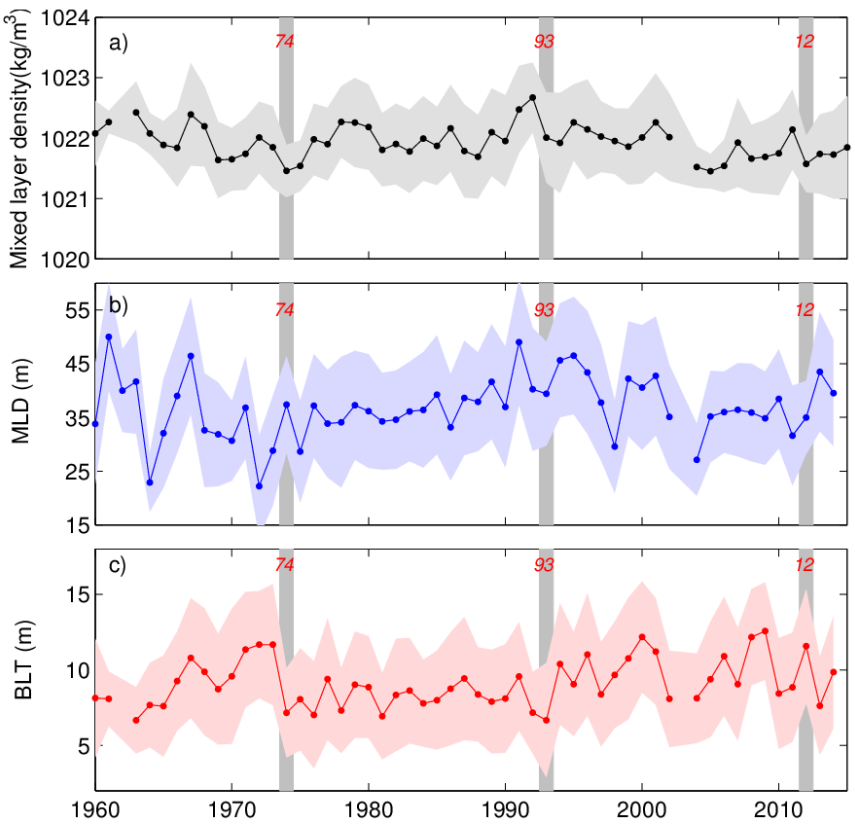

Figure 16. Time series of yearly (a) mixed layer density, (b) mixed layer depth, and (c) BLT averaged in the SCS. Error bars are shown in light shading. The gray shaded areas indicate turning points in 1974, 1993, and 2012.